Article

Photocorrosion Inhibition and Enhancement of Photocatalytic Activity for ZnO via Hybridization with C

Hongbo Fu, Tongguang Xu, Shengbao Zhu, and Yongfa Zhu

Environ. Sci. Technol., **2008**, 42 (21), 8064-8069 • DOI: 10.1021/es801484x • Publication Date (Web): 04 October 2008

Photocorrosion Inhibition and Enhancement of Photocatalytic Activity for ZnO via Hybridization with C_{60}

HONGBO FU,*,†,‡ TONGGUANG XU,† SHENGBAO ZHU,† AND YONGFA ZHU*,†

Department of Chemistry, Tsinghua University, Beijing 100084, P. R. China, and Department of Environmental Science and Engineering, Fudan University, 220 Handan Road, Shanghai 200433, P. R. China

Received May 29, 2008. Revised manuscript received August 02, 2008. Accepted August 14, 2008.

C_{60} molecules with monomolecular layer state dispersed on the surface of ZnO and formed the hybridized interaction between ZnO and C_{60}. C_{60}-hybridized ZnO photocatalyst showed enhanced photocatalytic activity for the degradation of the organic dye and the photocorrosion of ZnO was successfully inhibited by the hybridization of C_{60} molecules. The photocorrosion inhibition of ZnO by C_{60} molecule could be attributed to the reduced activation of surface oxygen atom. The enhanced photocatalytic activity for C_{60}-hybridized ZnO was originated from the high migration efficiency of photoinduced electrons on the interface of C_{60} and ZnO, which was produced by the interaction of C_{60} and ZnO with a conjugative π-system. The enhancement degree of photocatalytic activity was strongly depended on the coverage of C_{60} molecules on the surface of ZnO nanoparticles, and the optimum hybridization effect was found at a weight ratio of 1.5% (C_{60}/ZnO). The hybridization of C_{60} with semiconductors could be used to improve the photocatalytic activity as well as the photostability.

1. Introduction

Photocatalysis has been widely applied as techniques of destruction of organic pollutants. Up to now, TiO_2 has been extensively investigated as one of the most active semiconductor photocatalysts (*1*). A major limitation of achieving high photocatalytic efficiency is the quick recombination of charge carriers. Recombination, which has faster kinetics than surface redox reactions, is a major drawback as it reduces the quantum efficiency of photocatalysis. Therefore, it is an important way to promote the photocatalysis efficiency by decreasing the recombination rate. ZnO with higher photocatalytic efficiency than TiO_2 holds the drawback of photocorrosion effect during light irradiation and causes the decrease in photocatalytic activity and stability (*2*).

Considering that photochemical reactions mainly take place on the surface of the catalyst, surface modification has been recognized as one of the most intriguing methods to build the excellent photocatalyst (*3*). Surface modification may change the charge, functionality, reactivity of the surface, and enhance stability. Several attempts have been made to reduce the recombination of photoinduced hole−electron pairs during the photocatalytic reactions by surface modification (*4*). Among these surface modification methods, TiO_2 has been conjugated with electron scavenging agents such as metals or organic molecules and carbon nanotube. Anatase TiO_2 coated with multiwall carbon nanotubes (MWNT) achieved twice the efficiency of a commercial photocatalyst (P25) for inactivation of bacterial endospores (*5*).

Fullerenes with their variety of interesting properties due to their unique electronic properties have been gained a lot of attention (*6*). It has been reported that fullerenes contain an extensively conjugated three-dimensional π system. C_{60}, for example, is described as having a closed-shell configuration consisting of 30 bonding molecular orbital with 60 π-electrons, which is suitable for the efficient electron transfer reduction because of the minimal changes of structure and salvation associated with electron transfer (*7*). It has been suggested that intramolecular photoprocesses (electron or energy transfer) can occur between the peripheral C_{60} subunits and the central core. Some results have demonstrated that fullerene can efficiently cause a rapid photoinduced charge separation and a relatively slow charge recombination (*7, 8*). Although use of fullerenes for scavenging photogenerated electrons from TiO_2, little attempt has been made to utilize the unique properties of fullerenes to increase the efficiency of photocatalysis. Judging from the excellent photocatalyst of ZnO and the efficient electron transfer property of C_{60}, combination of ZnO and C_{60} seems to be ideal for fulfilling enhanced photon efficiency. It is expected that the surface coating of ZnO with a preferred C_{60} material enables us to construct fullerene-based ZnO catalyst, not only to obtain higher efficiency, but also to avoid the photocorrosion of ZnO.

In this work, ZnO photocatalyst with monolayer coverage of C_{60} shows enhanced activity and excellent photostability for the degradation of methylene blue (MB). The possible mechanisms of photocorrosion inhibition and enhancement of photocatalytic activity via hybridization have been established in detail.

2. Experimental Section

2.1. Materials Preparation. High-purity (99.9%) C_{60} sample was supported by Beijing University. Particulate ZnO (particle diameter 10−20 nm, surface area 57.3 $m^2\ g^{-1}$) were commercial available. All chemicals used were reagent grade without further purification. C_{60}-hybridized ZnO sample was prepared as follows: an appropriate amount of C_{60} was added into toluene and sonicated for 30 min to make C_{60} disperse totally. ZnO powder (1 g) was added into the above solution and stirred for 24 h. An opaque powder was obtained after evaporated at 80 °C for 10 h. C_{60}-hybridized ZnO samples with other different mass ratio from 0.5 to 2.5% were prepared by following the same procedure as above. To test the photoelectrochemical performance of C_{60}-hybridized ZnO sample, the dispersed in ethanol solution sample was evenly spread onto an ITO (indium tin oxide) glass substrate with a sheet resistance of 15 Ω. After being dried, the ITO glass was calcined for 0.5 h at 200 °C in N_2 flow.

2.2. Characterization. High resolution transmission electron microscopy (HRTEM) images were obtained by JEM 2010F field emission transmission electron microscope with an accelerating voltage of 200 kV. X-ray diffraction (XRD) patterns of the powders were recorded at room temperature by a Bruker D8 Advance X-ray diffractometer. The diffuse reflectance absorption spectra (DRS) of the samples were

* Address correspondence to either author. Fax: +86-10-6278-7601 (Y.Z. and H.F.) E-mail: zhuyf@tsinghua.edu.cn (Y.Z.); fuhb@fudan.edu.cn (H.F.).
† Tsinghua University.
‡ Fudan University.

10.1021/es801484x CCC: $40.75
Published on Web 10/04/2008

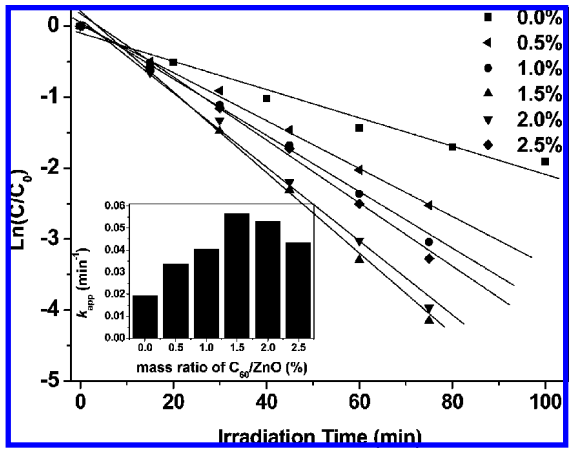

FIGURE 1. Photocatalytic degradation of MB over the as-prepared samples under UV-light irradiation (λ = 254 nm); catalyst loading, 0.5 g L^{-1}; MB, 1 × 10^{-5} M; Inset: effect of the C_{60} loading on the apparent rate constant (*k*).

recorded on a UV-visible spectrophotometer (Hitachi UV-3100) equipped with an integrated sphere attachment, and the spectra were recorded in the range of 200−800 nm. The Brunauer−Emmett−Teller (BET) surface area measurements were performed by a micromeritics (ASAP 2010 V5.02H) surface area analyzer. The nitrogen adsorption and desorption isotherms were measured at 77 K after degassing the samples on a Sorptomatic 1900 Carlo Erba Instrument. Raman spectra were recorded on a microscopic confocal Raman spectrometer (Renishaw 1000 NR) with an excitation of 514.5 nm laser light. Electrochemical and photoelectrochemical measurements were performed in a homemade three electrode quartz cells. Pt sheet was used as counter and Hg/Hg_2Cl_2/sat. KCl used as reference electrodes, whereas the working electrode was the thin film on ITO for investigation. The photoelectrochemical experiment results were recorded with a CHI 660B electrochemical system. The intensity of light was 1 mW cm^{-2}.

2.3. Photocatalytic Experiments. The photocatalytic activities of the as-prepared samples for the degradation of methylene blue (MB) in solution were tested under UV light. Methylene blue (MB), a typical dye contaminant in wastewater, is a blue cationic thiazine dye with maxima of absorbance at 660 (the most prominent), 614, and 292 nm. It has often been used as a model compound to test the photocatalytic degradation of organic materials. An 8 W UV lamp (λ = 254 nm,) was used as light resource, and the average light intensity was 150 $\mu W \cdot cm^{-2}$. 50 mg of C_{60}-hybridized ZnO photocatalysts were dispersed in a 100 mL MB suspension (1 × 10^{-5} M). Prior to the irradiation, the suspensions were magnetically stirred in the dark for 30 min to reach the absorption−desorption equilibrium. At given time intervals, 3 mL of the aliquots were sampled and analyzed by recording variations in the absorption band (665 nm) in the UV−visible spectra of MB using a Hitachi U-3010 UV-vis spectrophotometer.

3. Results and Discussion

3.1. Enhancement of Photocatalytic Activity. The photocatalytic activities of the C_{60}-hybridized ZnO samples were evaluated by the degradation of MB in aqueous solution, and the results are shown in Figure 1. The pseudo first-order relationship was revealed by the plots of $\ln(C/C_0)$ vs irradiation time (*t*). The blank test confirmed that MB was not degraded in the dark in the presence of the catalyst or irradiated under UV light at the absence of the catalyst. However, 85% of MB can be photodegraded by ZnO under UV irradiation for 75 min. All the hybridized ZnO samples exhibited higher photocatalytic activities than the pure ZnO sample. The sample with 1.5% of C_{60} showed the highest activity, 95% of MB can be photodegraded under the same conditions. The photocatalytic activity of ZnO hybridized by C_{60} can be enhanced by about 3 times compared to the ZnO sample. This result implied that the interaction between C_{60} and ZnO photocatalyst played a crucial role in the enhanced photocatalytic activity of ZnO semiconductor. The influence of amounts of C_{60} hybridized upon the photodegradation rate of MB is shown in the inset of Figure 1. One can see the loading amount of C_{60} presented a great influence on the photocatalytic activity of the as-prepared samples. The apparent reaction rate constant *k* was 0.0337, 0.0391, 0.0569, 0.0537, 0.0417, and 0.0188 min^{-1}, respectively, for the C_{60}/ZnO ratio of 0.5%, 1.0%, 1.5%, 2.0%, 2.5% and the pure ZnO sample. When the loading amount was below 1.5%, the photocatalytic activities enhanced with the increasing of loading amount of C_{60}. However, when the loading amount of C_{60} exceeded 1.5%, the photocatalytic activities of samples decreased as the amount of C_{60} increased. The optimal loading amount of C_{60} on the surface of ZnO nanoparticles was 1.5%. It can be explained that C_{60} tended to aggregate on the surface of ZnO when the mass ratio of C_{60} was above 1.5%, resulting in the slower transformation of the photoinduced electrons.

3.2. Photocorrosion Inhibition of ZnO Photocatalysts. To evaluate the photostability of the catalyst, the recycled experiments for the photodegradation of MB were performed, and the results are shown in Figure 2. 85% of MB could be degraded when ZnO was used for the first time, however, after three recycles, a significant decrease of photocatalytic activity for pure ZnO was found (Figure 2A), only 41% of MB was degraded within 80 min. After exposure under UV light for 50 h, there was almost no evident photocatalytic activity of ZnO for the MB photodegradation, and only 12% of MB could be degraded even after 80 min. The drastic decrease of photocatalytic activity for ZnO was resulted from the photocorrosion effect. While, after ZnO photocatalyst was hybridized by C_{60}, the recycled usage for three times did not affect its photocatalytic activity apparently. Even after irradiation under UV light for 50 h, the C_{60}-hybridized ZnO photocatalyst did not exhibit any significant decrease of photocatalytic activity (Figure 2B). Apparently, the photocorrosion effect of ZnO was inhibited by C_{60} molecules after hybridized. In this system, the presence of C_{60}-hybridized on the surface of ZnO enhanced the stability of the catalyst greatly (*9*).

The morphologies of the samples before and after photocatalysis were also observed (Supporting Information Figure S1). ZnO sample consisted of agglomerated approximately spherical particles with the diameter of 20 nm. Due to the less amount of C_{60} on the surface of ZnO nanoparticles, there was no change for the morphologies of ZnO. After the photocatalytic reaction, the spherical ZnO particles can not be seen and only web-like morphologies existed, indicating that the structure of the ZnO crystal has already changed. However, in the presence of the C_{60}, the morphology of ZnO was remained. The TEM result was in good agreement with the results of the circled photochemical experiment, further indicating that the photocorrosion effect of ZnO was inhibited by hybridized C_{60} molecular on its surface.

3.3. Hybrid Structure. The diffuse reflectance absorption spectra of the as-prepared sample with different mass ratios of C_{60}/ZnO are shown in Figure 3. C_{60}-hybridized ZnO with different mass ratios exhibited the visible absorption in the region from 400 to 800 nm. Compared with the pure ZnO, C_{60}-hybridized ZnO showed the same absorbance edge, but extended the absorbance to the visible region. The absorption intensity of the prepared samples changed with the increasing of the C_{60} amount. The absorption intensity increased rapidly

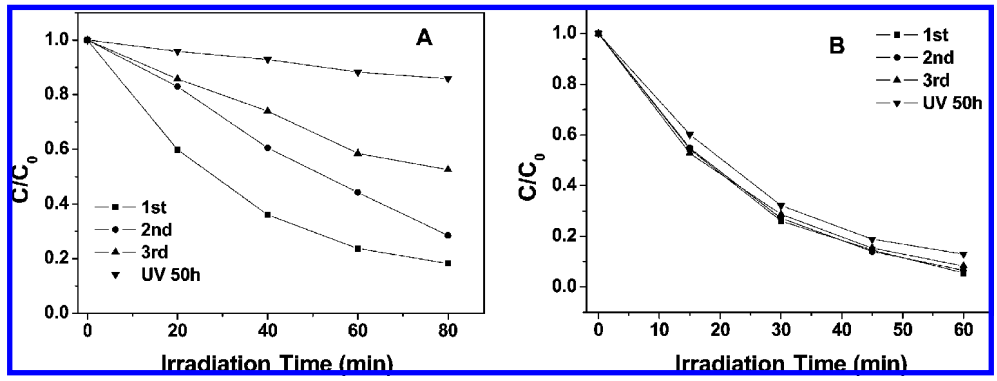

FIGURE 2. The circled photochemical experiment to observe the photostability of the as-prepared samples.

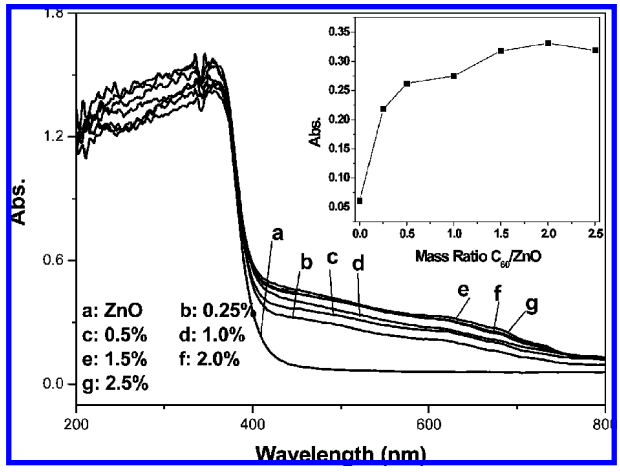

FIGURE 3. DRS of ZnO hybridized by C_{60} with the different ration of ZnO and C_{60}.

with the ratio of C_{60}/ZnO from 0.5 to 1.5%, but the increment was insignificant from 1.5 to 2.5%. Furthermore, the absorbance of samples at the wavelength of 600 nm changed with a function of mass ratio of C_{60}/ZnO (the inset of Figure 3). Considering the diameter of C_{60} (0.71 nm) and BET surface area of ZnO (57.3 m^2 g^{-1}), it was estimated that the weight ratio at which nearly compact C_{60} monolayer coverage was formed on the surface of ZnO was about 2%; the actual ratio of C_{60} absorbed on the surface of ZnO could be less than 2% because C_{60} can only occupy the active absorption site on the surface of ZnO. Based on the DRS observation, the absorption intensity almost remained unchanged when the ratio of C_{60}/ZnO increased from 1.5 to 2.5%, indicating that C_{60} may aggregate to form cluster on the surface of ZnO nanoparticles when the weight ratio of C_{60}/ZnO was above 1.5%.

The morphologies of the as-prepared sample (1.5% of C_{60}, w/w) were observed using HRTEM (Supporting Information Figure S2). The lattice spacing of approximately 0.341 nm between adjacent lattice planes corresponded to the distance between (200) crystal planes of ZnO (*10*). It was found that there was no change of lattice structure of ZnO after hybridized by C_{60} molecules. However, the outer boundary of the as-prepared sample was distinctly different from the pure ZnO. A coverture layer with noncrystal structure surrounded the surface of ZnO crystal. The thickness of the coverture layer was about 1 nm, which was close to the diameter of C_{60} molecular. It can be speculated the outer layer could be C_{60} molecule, which dispersed on the surface of ZnO with a monolayer structure. This estimation is based on the assumption that each C_{60} molecule occupies approximately 100 Å, and is spread evenly on the ZnO surface (*11*).

The existence of fullerene in the composite materials was also studied by Raman spectroscopy. As shown in Figure 4A, all the Raman shifts of free fullerenes can be found: Hg(1) (270 cm^{-1});Hg(2) (432 cm^{-1}); Ag(1) (494 cm^{-1}); Hg(3) (707 cm^{-1}); Hg(4)(770 cm^{-1}); Hg(7) (1420 cm^{-1}); Ag(2) (1464 cm^{-1}) (*12*). It was clear that some changes occurred in the Raman spectrum after C_{60} was hybridized with ZnO, the Ag(2) symmetry band at 1464 cm^{-1} was slightly downshifted and broadened with the doping amount of C_{60} increasing. This most characteristic Raman band at 1464 cm^{-1} for the Ag(2) pentagonal pinch mode was related to the carrier transfer. When there is charge transfer to C_{60} molecules, the mode would shift to the low frequency region. From the results of downshifts for 1464 cm^{-1}, it can be concluded that partial electron transfers from ZnO to the C_{60} molecules. At low coverage, the Ag(2) mode appearedat about 1464 cm^{-1},which was similar with that of pure C_{60}. As the coverage increased, the mode was downshifted to the low frequency. As the coverage of C_{60} further increasing, the hybridization interaction between ZnO and C_{60} become weaker. This can be explained that at the coverage of 1.5%, the C_{60} molecules dispersed on the surface of ZnO with near-monolayer molecular states, stronger hybridization interaction was present. When the coverage was above 1.5%, the aggregation of C_{60} molecules occurred on the surface of ZnO and formed C_{60} clusters, resulting in the decrease of hybridization interaction between ZnO and C_{60}. The interaction between C_{60} and ZnO can also be revealed by infrared spectroscopy. The IR spectrum of ZnO, C_{60}, and the C_{60}-hybridized ZnO photocatalyst (1.5%) are shown in Figure 4B. The peaks at 527, 577, 1183, and 1428 cm^{-1} are attributed to the internal modes of the C_{60} molecule (*13*). The hybridization between ZnO and C_{60} molecules resulted in some changes in the IR spectrum of C_{60}. It could be found that the characteristic mode at 1182 cm^{-1} split into two peaks at about 1229 and 1162 cm^{-1}. These two characteristic modes (1182 cm^{-1} and 1428 cm^{-1}) are known for being sensitive to charge transfer of C_{60}, therefore, it can be concluded that the occurrence charge-transfers from ZnO to C_{60} inducing the splitting and extension, the interaction by hybridization effect existed between ZnO and C_{60} (*14*)

The pore size distributions were measured by BJH desorption isotherms (Supporting Information Figure S3). There was no appreciable change for the surface area before (57.3 m^2 g^{-1}) and after hybridization (56.9 m^2 g^{-1}) by C_{60}. The above results implied that the modification of C_{60} did not obviously change the pore structure of ZnO photocatalyst. Based on all the above results, it could be concluded that C_{60} molecule was bonded on the surface of ZnO forming a monomolecular layer, and there existed an intimate contact and interaction between C_{60} and ZnO phase.

3.4. Photoelectric Properties. The photoelectrochemical performance of the as-prepared samples was also studied. The photoelectrochemical response of ITO/ZnO and ITO/

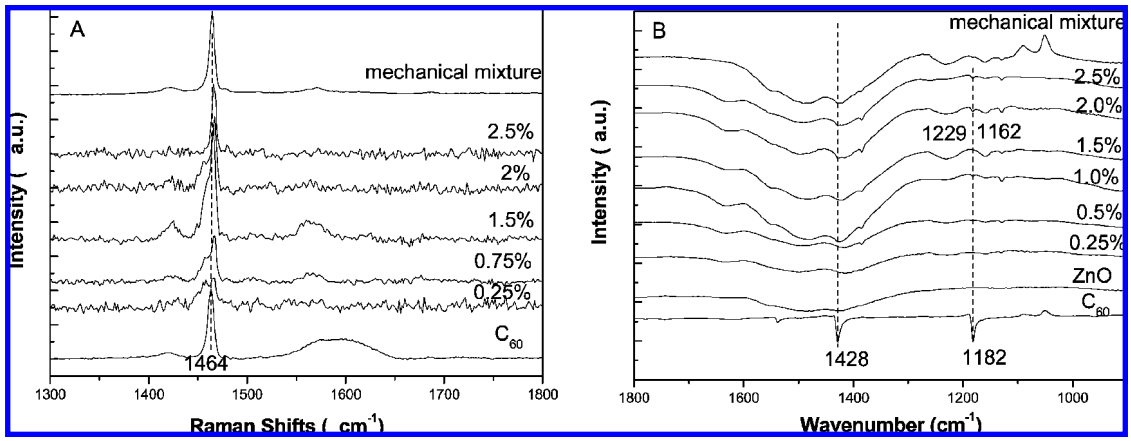

FIGURE 4. Laser Raman Spectroscopy (A) and FTIR (B) of C_{60}, ZnO and C_{60} hybridized ZnO photocatalyst.

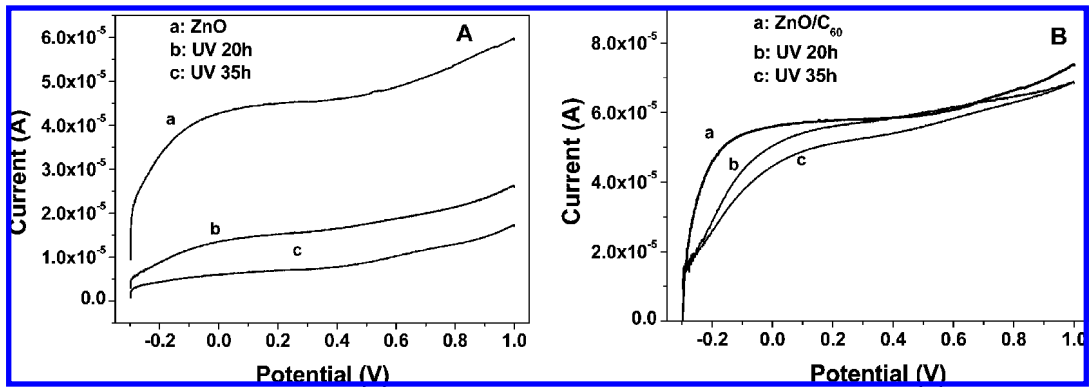

FIGURE 5. Current−potential plots recorded for ZnO film (A) and C_{60}- hybridized ZnO film (B).

ZnO/C_{60} thin films vs bias potential are shown in Figure 5. With the increase of bias potential, the photocurrent of both ITO/ZnO and ITO/ZnO/C_{60} thin films increased. Under the same bias potential, the photocurrent of C_{60}-hybridized ZnO was higher than that of pure ZnO film. The photocurrent enhancement of C_{60}-hybridized ZnO indicated a higher separation efficiency of photoinduced electron and hole, which could be due to the interaction of C_{60} molecule layer and ZnO semiconductor. In the case of the ZnO film, the photocurrent of the film decreased dramatically when exposed to UV light for 20 h. With the exposure increased to 35 h, the photoelectrochemical response further decreased (Figure 5A). In contrast, no significant difference could be observed when the C_{60}-hybridized ZnO film was exposed to UV light for a long time (Figure 5B). This could be due to the enhanced photostability of ZnO in the presence of the coverage of C_{60} monomolecular layer.

The potential of working electrode was set at 0.0 V versus Pt counter electrode, and the photocurrent response with the irradiation time was also observed (Supporting Information Figure S4). The initial photocurrent of C_{60}-hybridized ZnO film was apparently stronger than that of the pure ZnO film. When irradiated for 20 h, the photocurrent of C_{60}-hybridized ZnO film decreased slightly from 4.54×10^{-5} to 3.50×10^{-5} A. With the reaction further proceed from 20 to 70 h, the photocurrent of the sample kept invariable. As for the pure ZnO film, the photocurrent decreased sharply from 3.45×10^{-5} to 0.92×10^{-5}A. Almost no photoelectrochemical response could be observed when it was irradiated for 70 h. All these results proved that the combination of ZnO nanoparticles and C_{60} molecules was an effective way to improve photon efficiency, as well as to enhance the photostability of ZnO.

A typical EIS response of illuminated C_{60}-hybridized ZnO electrodes obtained in the presence of Na_2SO_4 (0.1M) is present in Supporting Information Figure S5. In each case, there was only one arc/semicircle on the EIS plane display, suggesting that only the surface charge-transfer step is in the photocatalytic reaction (*15*). The smallest arc radius on the EIS Nyquist plot means an effective separation of the photogenerated electron−hole pair and a fast interfacial charge transfer to the electron donor/electron acceptor. The arc radius at high frequency was largely decreased and increased gradually with the amount of C_{60} hybridized on the surface of ZnO. It was also found that the order of arc radius order was consistent with the order of photocatalytic activities, reflecting the difference of interfacial charge transfer for different hybridized electrodes (*15*).

3.5. The Proposed Mechanism. The photocatalytic activity of C_{60}-hybridized ZnO (1.5%) significantly differed from that of the pure ZnO. As a reference, a mechanical mixture of C_{60} and ZnO sample (1.5% of C_{60}, w/w) was prepared by stirring merely, its photocatalytic activity was similar to that of the pure ZnO sample, and much lower photocatalytic activity compared with 1.5% C_{60}-hybridized ZnO catalyst, which indicated that the C_{60} adsorbed could interact strongly with ZnO surface, and produced a hybridized form. Such interaction could be responsible for the enhanced photocatalytic activity of ZnO, since the hybridization of C_{60} did not change the crystal structure of ZnO (Supporting Information Figure S2). The formation of an associated complex in colloidal semiconductor systems is not unusual (*16*). The ability of two different kinds of semiconductor (e.g., TiO_2−CdS and ZnO−CdS) to interact with each other, and participate in the charge transfer process has been demonstrated. Moreover, the electronic properties of these systems (ZnO, TiO_2, or C_{60}) are such that they can readily undergo charge transfer interaction with electron acceptors or donors. The complexation of TiO_2 surface with molecules having electron donor groups such as carboxylate and thiocyanate and of C_{60}

with amines has been reported (*17*). Although no direct proof were supplied, it was evident from the present results that the hybrid between C_{60} and ZnO was responsible for the efficient charge transfer process under UV excitation, which was especially marked when the hybridized C_{60} was present as a monomolecular layer coverage.

Photodegradation of chemicals with ZnO photocatalyst have been studied previously (*18*). When a UV photon is absorbed by a wide-band gap semiconductor ZnO, an e^-/h^+ pair is generated. The e^- and h^+ could migrate to the surface to react with the adsorbed reactants in the desired process, or they could undergo a nondesired recombination. A rate increase in the former process or a rate decrease in the latter would lead to greater photocatalytic efficiency. It has been reported that the delocalized conjugated π structure of C_{60} made it easier to transfer the photoinduced electrons (*19*). In the present system, the energy of conduction band (CB) of ZnO (ECB ≈ -0.5 V vs NHE at pH 7) thermodynamically favor electron-transfer (E (C_{60}/C_{60}^- ≈ -0.2 V vs NHE) (*20*). The intrinsic excitation of ZnO nanoparticle photocatalyst with 254 nm UV light results in the charge separation. The photogenerated electron could be easily transferred to C_{60}, leading to a rate decrease in the recombination of photogenerated electron and hole (*21*). In the air-saturated solution, the back electron transfer between the ejected electron and $ZnO^{\bullet+}$ is suppressed for the dissolved oxygen scavenges electrons. On this step the superoxide radicals $O_2^{\bullet+}$ generates. As a result, the transfer of electron from CB of ZnO could proceed endlessly by this route. Although the five electrons can be accumulated by successive transfer on the surface of C_{60}, the primary step of charge transfer from excited ZnO into C_{60} is expected to involve only one-electron transfer. This is considered on the basis of the conduction band (ECB ≈ -0.5 V vs SCE at pH 8) and the reduction potential of C_{60} for one-electron reduction ($E = -0.36$ V vs SCE). Since further reductions of C_{60} can be carried out only at more negative potentials (< -0.83 V vs SCE), multiple transfer of electron from the CB of ZnO to C_{60} surface is not thermodynamically feasible in the ZnO/C_{60} system (*21*).

Although valence band holes are energetic enough to oxidize C_{60}, the contribution of this process is expected to be negligible because the presence of high concentration of the dye competes more effectively in the scavenging process of hole (*22*). It should be noted that the high excited states ignited by a photon will be energetic enough to inject electron into the semiconductor. Kamat et al. have reported that the excited C_{60} could transfer an electron to TiO_2 surface under visible-light irradiation. Under such condition, the pulse duration of the laser pulse (6 ns) is sufficiently long enough for the S_1 state of C_{60} to get excited into higher electronic states, and induce the photoinjection process (*23*). However, photoinjection of electrons from excited C_{60} into ZnO is unlikely under the present condition. As mentioned previously, a mercury lamp was used as the light source, and the UV light ($\lambda = 254$ nm) was supplied. It has been demonstrated that photons with such energy could not excite C_{60} to a higher electronic states (*24*).

Beyond the higher photocatalytic efficiency, the presence of C_{60} significantly enhanced the photostability of ZnO nanocrystalline. In the past, there is much evidence to suggest that ZnO semiconductor suffers from the photoinduced dissolution which greatly decreases its photocatalytic activity (*25*). This photocorrosion process of the ZnO semiconductor can be represented as follows:

$$ZnO + 2h^+ + nH_2O \rightarrow Zn(OH)n^{(2-n)+} + 1/2O_2 + nH^+ \quad (1)$$

where n depends on the pH of the solution. According to Gerischer's report, the sequence of steps involved in the photodecomposition of ZnO crystals consists of two slow steps where two holes are trapped on the surface, followed by the fast formation of an oxygen molecule and the fast expulsion of Zn^{2+} from the surface (*26*), i.e.,

$$O^{2-}_{surface} + h^+ \rightarrow O^-_{surface} \quad (2)$$

$$O^-_{surface} + 3\ O^{2-} + 3h^+ \rightarrow 2(O{-}O^{2-}) \quad (3)$$

$$O{-}O^{2-} + 2h^+ \rightarrow O_2 \quad (4)$$

$$2\ Zn^{2+} \rightarrow 2\ Zn^{2+}(aq) \quad (5)$$

The overall reaction may be represented as

$$ZnO + 2h^+ \rightarrow Zn^{2+} + 1/2\ O_2 \quad (6)$$

It is well-known that ZnO is a highly doped *n*-type defect semiconductor ($Zn_{1+\sigma}O$ where $\sigma > 0$) with the principal defect being the zinc interstitial (*27*). As a result, the bond of oxygen atoms on the surface of ZnO exists as the unsaturated state. When ZnO nanoparticles are subjected to intrinsic excitation, electrons are promoted from the valence to the conduction band generating electron−hole pair separation. The holes are transported to the solid-solution interface and are prone to undergoing a reaction with surface oxygen atom, resulting in the escape of oxygen from the surface. In this process, the photocorrosion of ZnO consume some photoinduced holes, which damage the photocatalytic activity of ZnO. Furthermore, the crystal structure of ZnO collapses, and loses the activity for the MB degradation ultimately. When C_{60} is introduced on the surface of ZnO, these vacant sites could play the role of anchor sites for the C_{60} molecule. Thus, the adsorption processes substantially reduce the activation of surface oxygen atom, and effectively inhibit the photocorrosion of ZnO.

The photocatalysts were gained from the suspension by a simple filtration and then observed by XRD. For comparison, XRD patterns of the samples before and after irradiation were measured together under the same condition, and the results are shown in Supporting Information Figure S6. All the diffraction peaks can be indexed as the hexagonal ZnO with lattice constants $a = 3.249$ Å and $c = 5.206$ Å, which were consistent with the JCPDS 36−1451. XRD pattern showed that no change could be found when ZnO was hybridized by C_{60}, indicating the hybridization of C_{60} did not influence the lattice structure of ZnO. No diffraction peak assigned to C_{60} can be found due to the less amount of C_{60} loading on the surface of ZnO catalyst. When exposed to UV light, all the diffraction peaks of pure ZnO sample decreased swiftly, and the new diffraction peaks appeared, which was assigned to the $Zn_5(OH)_6(CO_3)_2$ phase, suggesting that the crystal structure of ZnO was changed. However, the XRD pattern of C_{60}-hybridized ZnO varied insignificantly after irradiation. The enhanced stability of ZnO observed in this study could be attributed, almost solely, to the presence of C_{60} coverage.

Acknowledgments

This work is supported by the National Natural Science Foundation of China (20673065, 20747002) and National Basic Research Program of China (2007CB613303).

Supporting Information Available

TEM, HRTEM, BJH pore size distribution plots, EIS of the pure ZnO and the C_{60} hybridized ZnO sample, XRD patterns of the samples before and after the photocatalysis experiment. This material is available free of charge via the Internet at http://pubs.acs.org.

Literature Cited

(1) Hoffmann, M. R.; Martin, S. T.; Choi, W.; Bahnemann, D. W. Environmental applications of semiconductor photocatalysis. *Chem. Rev.* **1995**, *95*, 69–96.

(2) (a) Ye, C.; Bando, Y.; Shen, G.; Golberg, D. Thickness-dependent photocatalytic performance of ZnO nanoplatelets. *J. Phys. Chem. B* **2006**, *110*, 15146–15151. (b) Cao, B.; Cai, W. J. From ZnO nanorods to nanoplates: chemical bath deposition growth and surface-related emissions. *J. Phys. Chem. C* **2008**, *112*, 680–685. (c) Li, Q.; Kumar, V.; Li, Y.; Zhang, H.; Marks, T. J.; Chang, R. P. H. Fabrication of ZnO nanorods and nanotubes in aqueous solutions. *Chem. Mater.* **2005**, *17*, 1001–1006.

(3) Noguchi, H.; Nakajima, A.; Watanabe, T.; Hashimoto, K. Design of a photocatalyst for bromate decomposition: surface modification of TiO_2 by pseudo-boehmite. *Environ. Sci. Technol.* **2003**, *37*, 153–157.

(4) Makarova, O. V.; Rajh, T.; Thurnauer, M. C.; Martin, A.; Kemme, P. A.; Cropek, D. Surface modification of TiO_2 nanoparticles for photochemical reduction of nitrobenzene. *Environ. Sci. Technol.* **2000**, *34*, 4797–4803.

(5) Lee, S. H.; Pumprueg, S.; Moudgil, B.; Sigmund, W. Inactivation of bacterial endospores by photocatalytic nanocomposites. *Colloids Surf. B* **2005**, *40*, 93–98.

(6) Haddon, R. C. Chemistry of the fullerenes: the manifestation of strain in a class of continuous aromatic-molecules. *Science* **1993**, *261*, 1545–1550.

(7) Hasobe, T.; Hattori, S.; Kamat, P. V.; Fukuzumi, S. Supramolecular nanostructured assemblies of different types of porphyrins with fullerene using TiO_2 nanoparticles for light energy conversion. *Tetrahedron* **2006**, *62*, 1937–1946.

(8) Zhu, S.; Xu, T.; Fu, H.; Zhao, J.; Zhu, Y. Synergetic effect of Bi_2WO_6 photocatalyst with C_{60} and enhanced photoactivity under visible irradiation. *Environ. Sci. Technol.* **2007**, *41*, 6234–6239.

(9) Brabec, C. J.; Cravino, A.; Meissner, D. Origin of the open circuit voltage of plastic solar cells. *Adv. Funct. Mater.* **2001**, *11*, 374–380.

(10) Kuo, C.-L.; Kuo, T.-J.; Huang, M. H. Hydrothermal synthesis of ZnO microspheres and hexagonal microrods with sheetlike and platelike nanostructures. *J. Phys. Chem. B* **2005**, *109*, 20115–20121.

(11) Schiiavello, M.; Augugliaro, V.; Palmisano, L.; Sclafani, A.; Venezia, A. M. Comments on the paper "Spectroscopic, photoconductivity, and photocatalytic studies of TiO_2 colloids: naked and with the lattice doped with Cr^{3+}, Fe^{3+}, and V^{5+} Cations. *Langmuir* **1995**, *11*, 3278–3278.

(12) Schettino, V.; Pagliai, M.; Ciabini, L.; Cardini, G. The vibrational spectrum of fullerene C_{60}. *J. Phys. Chem. A* **2001**, *105*, 11192–11196.

(13) Stepanian, S. G.; Karachevtsev, V. A.; Plokhotnichenko, A. M.; Adamowicz, L.; Rao, A. M. IR spectra of photopolymerized C_{60} films. Experimental and density functional theory study. *J. Phys. Chem. B* **2006**, *110*, 15769–15775.

(14) Kato, H.; Takemura, S.; Iwasaki, K.; Watanabe, Y.; Nanba, N.; Hiramatsu, T.; Nishikawa, O.; Taniguchi, M. X-ray photoemission spectroscopy and Fourier transform infrared characterizations of C_{60} states in C_{60} doped conducting polymers. *J. Vac. Sci. Technol.* **2006**, *A24*, 1500–1504.

(15) Leng, W. H.; Zhang, Z.; Zhang, J. Q.; Cao, C. N. Investigation of the kinetics of a TiO_2 photoelectrocatalytic reaction involving charge transfer and recombination through surface states by electrochemical impedance spectroscopy. *J. Phys. Chem. B* **2005**, *109*, 15008–15023.

(16) Gopidas, K. R.; Bohorquez, M.; Kamat, P. V. Photophysical and photochemical aspects of coupled semiconductors: charge-transfer processes in colloidal cadmium sulfide-titania and cadmium sulfide-silver(I) iodide systems. *J. Phys. Chem.* **1990**, *94*, 6435–6440.

(17) Nazeeruddin, M. K.; Kay, A.; Rodicio, I.; Humphry-Baker, R.; Muller, E. Conversion of light to electricity by cis-X2bis(2,2′-bipyridyl-4,4′-dicarboxylate)ruthenium(II) charge-transfer sensitizers ($X = Cl^-$, Br^-, I^-, CN^-, and SCN^-) on nanocrystalline titanium dioxide electrodes. *J. Am. Chem. Soc.* **1993**, *115*, 6382–6390.

(18) (a) Houskova, V.; Stengl, V.; Bakardjieva, S.; Murafa, N.; Kalendova, A.; Oplustil, F. Zinc oxide prepared by homogeneous hydrolysis with thioacetamide, its destruction of warfare agents, and photocatalytic Activity. *J. Phys. Chem. A* **2007**, *111*, 4215–4221. (b) Mai, F. D.; Chen, C. C.; Chen, J. L.; Liu, S. C. Photodegradation of methyl green using visible irradiation in ZnO suspensions: Determination of the reaction pathway and identification of intermediates by a high-performance liquid chromatography-photodiode array-electrospray ionization-mass spectrometry method. *J. Chromatogr., A* **2008**, *1189*, 355–365. (c) Chen, C. C. Degradation pathways of ethyl violet by photocatalytic reaction with ZnO dispersions. *J. Mol. Catal. A* **2007**, *264*, 82–92.

(19) Haddon, R. C. pi.-Electrons in three dimensions. *Acc. Chem. Res.* **1988**, *21*, 243–249.

(20) Kamat, P. V.; Bedja, I.; Hotchandani, S. Photoinduced charge transfer between carbon and semiconductor clusters. One-electron reduction of C_{60} in colloidal TiO_2 semiconductor suspensions. *J. Phys. Chem.* **1994**, *98*, 9137–9142.

(21) Kamat, P. V. Photoinduced charge transfer between fullerenes (C_{60} and C_{70}) and semiconductor zinc oxide colloids. *J. Am. Chem. Soc.* **1991**, *113*, 9705–9707.

(22) Mrowetz, M.; Balcerski, W.; Colussi, A.; Hoffmann, M. R. Oxidative power of nitrogen-doped TiO_2 photocatalysts under visible illumination. *J. Phys. Chem. B* **2004**, *108*, 17269.

(23) Krishna, V.; Noguchi, N.; Koopman, B.; Moudgil, B. J. Enhancement of titanium dioxide photocatalysis by water-soluble fullerenes. *Colloid Interface Sci.* **2004**, *304*, 166–171.

(24) Kamat, P. V.; Gevaert, M. Vinodgopal, K. Photochemistry on semiconductor surfaces. Visible light induced oxidation of C_{60} on TiO_2 nanoparticles. *J. Phys. Chem. B* **1997**, *101*, 4422–4427.

(25) Spathis, P.; Poulio, I. The corrosion and photocorrosion of zinc and zinc-oxide coatings. *Corros. Sci.* **1995**, *51*, 673–680.

(26) Rudd, A. L.; Bresli, C. B. Photo-induced dissolution of zinc in alkaline solutions. *Electrochim. Acta* **2000**, *45*, 1571–1579.

(27) Wang, D.; Song, C. Controllable synthesis of ZnO nanorod and prism arrays in a large area. *J. Phys. Chem. B* **2005**, *109*, 12697–12700.

ES801484X